Fusion of Multipath Data with ML-PMHT for Very Low SNR Track Detection in an OTHR

KEVIN ROMEO
YAAKOV BAR-SHALOM
PETER WILLETT

The Maximum Likelihood Probabilistic Multi-Hypothesis Tracker (ML-PMHT) is formulated for and applied to an Over-The-Horizon radar (OTHR) scenario. In this scenario there are two ionosphere layers acting as reflectors of the electromagnetic (EM) waves and each scan can contain multiple measurements (up to four) originating from each target; each of these target-originated measurements takes one of four possible round-trip paths. The ML-PMHT likelihood ratio is modified to model this uncertainty in the measurement path which then allows the fusion of multipath data in the presence of false measurements.

This tracker is shown to have a high track detection probability and track accuracy with a low probability of false track in very low signal to noise ratio (SNR) OTHR scenarios. It is also shown to be a statistically efficient estimator. Consequently, the ML-PMHT holds great promise in increasing the sensitivity and robustness of the next generation OTHR.

Results indicate that one can achieve for a very low observable (VLO) target a true track detection probability above 95% and a false track rate under one per 24 hours.

Manuscript received September 24, 2014; revised March 6, 2015; released for publication May 29, 2015.

Refereeing of this contribution was handled by Stefano Coraluppi.

Supported in part by ARO Grant W991NF-10-1-0369.

Authors' address: Dept. of Electrical and Computer Engineering, University of Connecticut, Storrs, CT 06269-4157 (e-mail: {romeo, ybs, willett}@engr.uconn.edu.)

1. INTRODUCTION

Over-the-horizon radar (OTHR) relies on signal refraction through the ionosphere to detect targets beyond the horizon. Due to the nature of the ionosphere, the signal from the radar may propagate via multiple paths, resulting in several target-originated detections. There is an ambiguity between detections and paths; the path corresponding to each target detection is not known. There are also measurements from false detections.

There are a wide range of approaches to the OTHR problem, varying in how detection, tracking, and association are handled. The multiple detection multiple hypothesis tracker (MD-MHT) [16] is formulated to solve the data association problem between measurements and measurement paths using an extended multiframe assignment technique. Alternatively, a multihypothesis fusion algorithm, presented in [11, 13–15], is a measurement-level fusion algorithm using only measurements already associated with targets by another filter to calculate the probabilities of association hypotheses. In [1, 2] a method is proposed for joint multiple target ground track estimation and slant track association. Additionally they assume unknown ionospheric conditions. Their method shows an improvement in accuracy and the number of correct track and path assignments. The Signal Inversion for Target Extraction and Registration (SIFTER) signal processing algorithm developed in [9] provides a better detection of low SNR targets in clutter by solving for the scattering surface that reproduces the radar's measurements and has been demonstrated effectively on real OTHR data.

Other approaches include applying the probabilistic data association filter (PDAF) [6–8], the multipath probabilistic data association algorithm (MPDA) [12], and the Probabilistic Multi-Hypothesis Tracker (PMHT) [8] to OTHR data. An extension of the PDAF called the Multiple Model Unified PDAF (MM-UPDAF) is developed in [7]. The MM-UPDAF is designed to handle multiple nonuniform clutter regions. The SNR in [7] is unavailable as the parameters used to determine the performance of the MM-UPDAF are proprietary. The lowest SNR available from [12] and [16] is around 10 dB, with an ionosphere model similar to what we use in our simulations. We show that our algorithm with a VLO target SNR of 4 dB yields a high track detection probability (95%) and a very low false track rate (less than one per day) for the scenario considered.

A multipath Expectation Maximization algorithm is developed and applied to an OTHR scenario in [10]. Similar to the PMHT, it treats data association as missing data. It also treats propagation paths as missing data. The (single path) Maximum Likelihood Probabilistic Multi-Hypothesis Tracker (ML-PMHT) uses the log-likelihood function based on the PMHT model. The ML-PMHT has previously been formulated for single and multitarget [17, 18] scenarios. It has been shown to perform well even with very low target SNR.

In this paper we extend the ML-PMHT formulation from [17, 18]. We present a generalized form of the ML-PMHT that accounts for multiple possible propagation paths. We apply this algorithm to an OTHR scenario. Unlike the MD-MHT [16], no data association is required. The ML-PMHT considers simultaneously all the measurements without knowing their origins or propagation paths and, remarkably, has *linear complexity in the number of measurements*. The ML-PMHT performs fusion of the multipath data in the presence of false measurements.

Section 2 briefly describes the ML-PMHT for a single target case and the extension to allow for multiple paths. Section 3 describes the multiple path extension to the ML-PDA. Section 4 presents the OTHR model used for simulation. Section 5 discusses the performance of the ML-PMHT from Monte Carlo testing. Section 6 develops the Cramér-Rao Lower Bound for the multipath ML-PMHT.

2. ML-PMHT

2.1. Single Target ML-PMHT

The ML-PMHT log-likelihood ratio (LLR) for the motion parameter of a single target is developed in [17]. This LLR is given by

$$\Lambda(\mathbf{x};Z) \triangleq \ln\left\{\frac{p(Z \mid \mathbf{x})}{p(Z \mid \text{all false})}\right\} = \sum_{i=1}^{N_w}\sum_{j=1}^{m_i} \ln\{\pi_0 + \pi_1 V p[\mathbf{z}_j(i) \mid \mathbf{x}(i)]\rho_j(i)\} \quad (1)$$

with

$$Z \triangleq \{\{\mathbf{z}_j(i)\}_{j=1}^{m_i}\}_{i=1}^{N_w} \quad (2)$$

Here N_w is the number of scans in the batch (the window length), and m_i is the number of measurements in the ith scan (frame). The parameter $\mathbf{x}$ determines the target state $\mathbf{x}(i)$ in a deterministic way (we use a constant velocity model[1] i.e., $\mathbf{x} = [s_t(1), \dot{s}_t]'$, where $s_t(1)$ and $\dot{s}_t$ are the initial position and velocity of the target, respectively). The prior probabilities that a measurement occurred due to clutter or due to a target are given by π_0 and π_1, respectively. These values are related to the probability of detection, P_D, and the probability of false alarm in a resolution cell, P_{FA}. The volume of the search region is V and a measurement, which didn't occur due to a target, has a uniform pdf in V. The jth measurement in the ith scan is $\mathbf{z}_j(i)$ and its associated amplitude likelihood ratio is $\rho_j(i)$. Finally, $p[\mathbf{z}_j(i) \mid \mathbf{x}(i)]$ is a Gaussian with mean determined by the target state parametrization $\mathbf{x}(i)$, and with the measurement noise covariance matrix. The amplitude likelihood ratio serves as a feature discriminant between the target originated measurements and the false ones due to spurious detections.

[1]Any arbitrary deterministic motion model can be used, such as deterministic motion in a known gravitational field [4].

The pdfs $p[Z(i) \mid \mathbf{x}(i)]$ (likelihood of the target present hypothesis) and $p[Z(i) \mid \text{all false}]$ (likelihood of the target absent hypothesis) are derived using the ML-PMHT assumptions [17]:

- There is a single target with known probability of detection.
- Any number of measurements in a scan can be assigned to the target.
- The motion of the target is deterministic.
- False detections are uniformly distributed.
- The number of false detections is Poisson distributed with known density.
- Amplitudes of target and false detections are Rayleigh distributed with known distribution.
- Target measurements are corrupted with zero-mean Gaussian noise.
- Measurements at different times, conditioned on the parameterized state, are independent.

These likelihoods are then given by

$$p[Z(i) \mid \mathbf{x}(i)] = \prod_{j=1}^{m_i}\left\{\frac{\pi_0}{V}p_0^\tau[a_j(i)] + \pi_1 p[\mathbf{z}_j(i) \mid \mathbf{x}(i)]p_1^\tau[a_j(i)]\right\} \quad (3)$$

$$p[Z(i) \mid \text{all false}] = \prod_{j=1}^{m_i}\frac{1}{V}p_0^\tau[a_j(i)] \quad (4)$$

where $p_0^\tau[a_j(i)]$ and $p_1^\tau[a_j(i)]$ are the pdfs of a false alarm and target measurement amplitude conditioned on exceeding the threshold τ, respectively.

2.2. The Multipath ML-PMHT Log-Likelihood Ratio for OTHR

The LLR of the generalized ML-PMHT that allows multiple propagation paths is given by

$$\Lambda(\mathbf{x};Z) = \sum_{i=1}^{N_w}\sum_{j=1}^{m_i}\ln\left\{\pi_0 + \pi_1 V \rho_j(i)\sum_{\ell=1}^{n_p} p[\mathbf{z}_j(i) \mid \mathbf{x}(i), \ell]P[\ell]\right\} \quad (5)$$

where ℓ is used to denote which path the signal took, $P[\ell]$ is the probability of path ℓ being taken, and n_p is the total number of possible paths. The mean of the Gaussian $p[\mathbf{z}_j(i) \mid \mathbf{x}(i), \ell]$ is $f_\ell(\mathbf{x}(i))$, where f_ℓ is the function that transforms the target state $\mathbf{x}(i)$ into the measurement space via path ℓ. The covariance matrix for this Gaussian is the measurement noise covariance for a measurement from path ℓ. Note that, for simplicity, we have assumed that $\rho_j(i)$ is the same for each path ℓ (a path dependent LLR can be used if available).

3. ML-PDA

We can extend the single-path ML-PDA likelihood presented in [17] to allow for multiple paths by applying

the total probability theorem. For a single scan this results in

$$\Lambda(\mathbf{x};Z) = \sum_{n_d=0}^{n_p} p(\mathbf{z} \mid \mathbf{x}, n_d) P(n_d) \tag{6}$$

$$P(n_d) = P_D^{n_d}(1-P_D)^{n_p-n_d}\binom{n_p}{n_d} \tag{7}$$

$$p(\mathbf{z} \mid \mathbf{x}, n_d) = \frac{1}{\binom{m}{n_d}\binom{n_p}{n_d} n_d!} \sum_{M\in\mathcal{M}_{n_d}} \sum_{A\in\mathcal{A}_{n_d}} \cdot p[\{\mathbf{z}_k\}_{k\notin M} \mid \text{“clutter”}] \prod_{j=1}^{n_d} p[\mathbf{z}_{M(j)} \mid \mathbf{x}, A(j)] \tag{8}$$

where n_d is the number of detections, and P_D is the probability of detection. $\mathcal{M}_{n_d}$ is the set of all unordered n_d-tuples of measurement indices. It contains $\binom{m}{n_d}$ n_d-tuples. $\mathcal{A}_{n_d}$ is the set of all ordered n_d-tuples of path indices. This set contains $\binom{n_p}{n_d} n_d!$ n_d-tuples. The ML-PDA gives similar results to the ML-PMHT in very low clutter scenarios, but is significantly more complex. For scenarios with a large amount of clutter (like the ones we are exploring in this paper) the ML-PDA becomes intractable due to the number of terms in the double summation in equation (8). Its CRLB is also complicated to determine since it requires extensive Monte Carlo simulations [5]. We choose the ML-PMHT for its simplicity and effectiveness. In a single scan i the ML-PMHT has $m_i n_p$ terms—linear complexity—while the ML-PDA has $\sum_{n_d=0}^{n_p}\binom{m_i}{n_d}\binom{n_p}{n_d} n_d! n_d = m_i n_p \sum_{n_d=0}^{n_p}(n_d-1)!\binom{m_i-1}{n_d-1} \cdot \binom{n_p-1}{n_d-1}$ terms and therefore suffers from a combinatorial explosion with increasing m_i.

4. OTHR MODEL

We investigate two two-dimensional OTHR scenarios which assume the target to be in a great circle plane on the earth's surface as shown in Figure 1, and a three-dimensional scenario where the target is on the surface of a sphere. We use a two-layer reflection model (spherical mirror model) for the ionosphere.[2] In this model the signal may reflect from either layer of the ionosphere resulting in multiple (up to four) round-trip propagation paths. In the 2-D and 3-D scenarios the radar measures slant range, slant range rate, and amplitude. In the 3-D scenario it also measures azimuth.

4.1. Measurement Amplitudes

We model the amplitudes of the measurements according to a Swerling I model [4]. The amplitude is

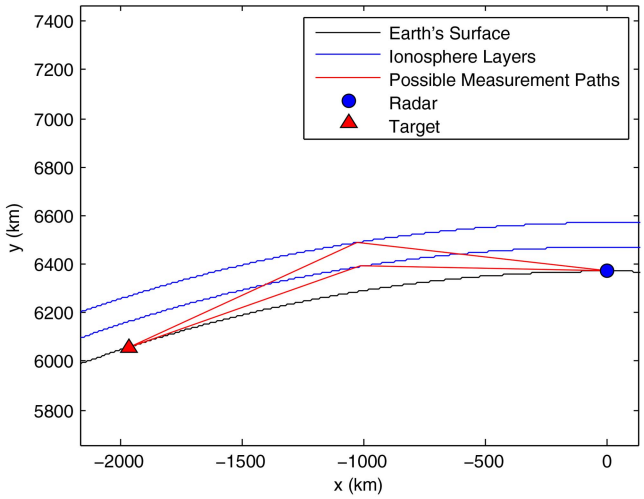

Fig. 1. The 2-D OTHR scenario with a reflection ionosphere model (spherical mirror model).

Rayleigh distributed with pdfs

$$p_0(a) = ae^{-a^2/2} \qquad a \geq 0 \tag{9}$$

$$p_1(a) = \frac{a}{1+d}e^{-a^2/2(1+d)} \qquad a \geq 0 \tag{10}$$

for the noise only and target, respectively. Here d is the expected SNR of the target in a resolution cell. For a chosen threshold τ we have

$$P_D = \int_\tau^\infty p_1(a)da \tag{11}$$

$$P_{FA} = \int_\tau^\infty p_0(a)da \tag{12}$$

The pdfs of the amplitude of a measurement given that it has exceeded the threshold τ are

$$p_0^\tau(a) = \frac{1}{P_{FA}}p_0(a) \qquad a \geq \tau \tag{13}$$

$$p_1^\tau(a) = \frac{1}{P_D}p_1(a) \qquad a \geq \tau \tag{14}$$

and the amplitude likelihood ratio is then

$$\rho_j(i) = \frac{p_1^\tau[a_j(i)]}{p_0^\tau[a_j(i)]} \tag{15}$$

4.2. Measurements

The OTHR measures both position and velocity of the target via slant range and slant range rate measurements. The equations of the measurements, given the signal reflected off the lower layer in both directions, are given below.[3] Defining

$$r_1 \triangleq 4\sqrt{h_1^2 - 2R_\oplus(h_1+R_\oplus)\cos\left(\frac{s_r-s_t}{2R_\oplus}\right) + 2h_1R_\oplus + 2R_\oplus^2} \tag{16}$$

[2]The actual paths are subject to refraction, which requires numerical algorithms for ray tracing. The reflection model used here is a simplified one, which, however, captures the essence of the OTHR.

[3]The signal propagates forward and is reflected in the plane of the great circle defined by the radar and the target. We assume that the antenna beam illuminating the target is in this plane. This beam corresponds to the measured azimuth of the reflection from the target.

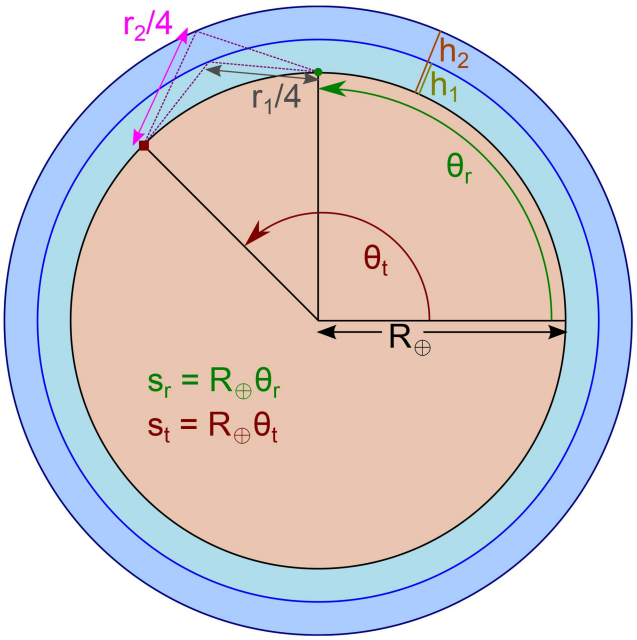

Fig. 2. Illustration of the geometry used to derive the equations for the measurements. Here θ_r and θ_t are the angles in polar coordinates of the radar and the target, respectively.

$$\dot{r}_1 \triangleq \frac{\partial r_1}{\partial s_t}\frac{\partial s_t}{\partial t} = -\frac{2\sin\left(\frac{s_r - s_t}{2R_\oplus}\right)(R_\oplus + h_1)}{\sqrt{2R_\oplus h_1 + 2R_\oplus^2 + h_1^2 - 2R_\oplus\cos\left(\frac{s_r - s_t}{2R_\oplus}\right)(R_\oplus + h_1)}}\dot{s}_t \tag{17}$$

one has

$$z_{r_1} = r_1 + w_{r_1} \tag{18}$$

$$z_{\dot{r}_1} = \dot{r}_1 + w_{\dot{r}_1} \tag{19}$$

Here h_1 is the height of the lower ionosphere layer. The radius of the earth is $R_\oplus$. The locations of the radar and target on the surface of the earth (on the great circle connecting them) are given by s_r and s_t, respectively. An illustration of the geometry of this problem is shown in Fig. 2. The velocity of the target along the great circle is $\dot{s}_t$. The noise terms, w_{r_1} and $w_{\dot{r}_1}$, are zero-mean, Gaussian, independent of each other, and with variances σ_r and $\sigma_{\dot{r}}$, respectively. We assume, for simplicity, the same noise variances on the other paths.

Given that the signal reflected off the upper layer only (with height h_2), we can find similar equations for r_2, $\dot{r}_2$, z_{r_2}, and $z_{\dot{r}_2}$, with noises w_{r_2} and $w_{\dot{r}_2}$. The equations for the measurements resulting from the remaining two paths, where the signal reflects off of alternate layers, can then be expressed as

$$z_{r_3} = \tfrac{1}{2}(r_1 + r_2) + w_{r_3} \tag{20}$$

$$z_{\dot{r}_3} = \tfrac{1}{2}(\dot{r}_1 + \dot{r}_2) + w_{\dot{r}_3} \tag{21}$$

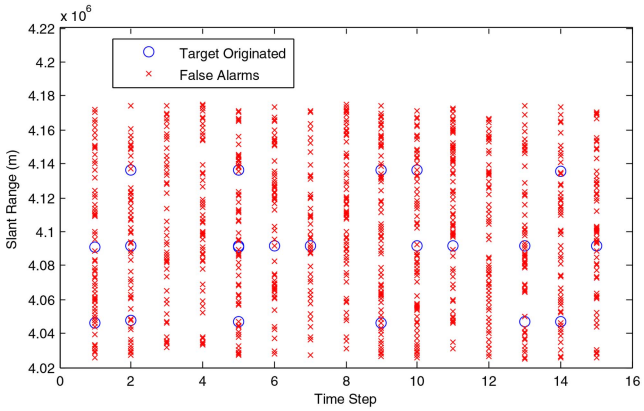

Fig. 3. Slant range measurements in one batch in 2-D scenario 1 (4 dB post-signal processing SNR).

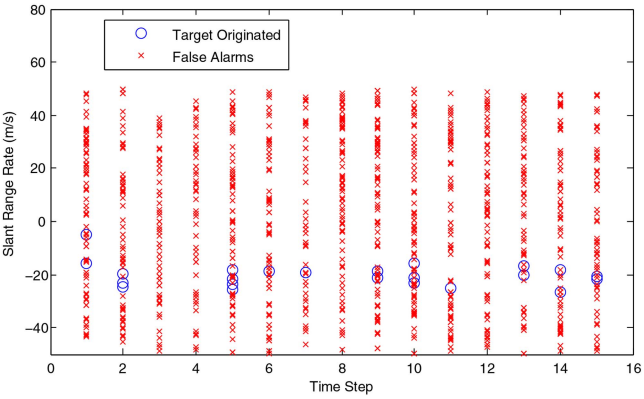

Fig. 4. Slant range rate measurements in one batch in 2-D scenario 1 (4 dB post-signal processing SNR).

$$z_{r_4} = \tfrac{1}{2}(r_1 + r_2) + w_{r_4} \tag{22}$$

$$z_{\dot{r}_4} = \tfrac{1}{2}(\dot{r}_1 + \dot{r}_2) + w_{\dot{r}_4} \tag{23}$$

The azimuth measurement (used only in the 3-D scenario) is given by

$$z_\theta = \theta + w_\theta \tag{24}$$

where θ is the true azimuth of the target, and the noise term w_θ is zero-mean, Gaussian, and has variance σ_θ.

4.3. 2-D Simulation Parameters

We simulated a target with an initial position 2000 km away from the radar, moving with a constant speed of 10 m/s towards it. The other values used in the 2-D simulations are given in Tables I and II. Figures 3 and 4 show the measurements used (after amplitude thresholding) in one run of the tracker from scenario 1. False measurements are generated uniformly in the measurement space. Note that, due to the very low SNR in a cell, P_D is a meager 0.34 and the high P_{FA} leads to 60 false measurements per scan. Also note that there are usually zero to three target originated measurements in each scan (rarely all four) and the overwhelming number of false measurements, which, however, can be

TABLE I
Scenario parameters used in the both the 2-D and 3-D simulations.

N_w	15
Time between scans	1 s
σ_r	300 m
$\sigma_{\dot{r}}$	5 m/s
SNR in a cell	**2.5 = 4 dB**
$R_\oplus$	6371 km
Ionosphere lower layer height	100 km
Ionosphere upper layer height	200 km
$P[\ell]$ for all ℓ	0.25

successfully handled by the multipath ML-PMHT track detector.

4.4. 3-D Simulation Parameters

We also simulated a target starting at 2000 km away from the radar and 0 azimuth. It is moving with a constant speed of 10 m/s with an initial course of 5°. The target follows the great circle starting from these initial conditions. The other values used in the 3-D simulation are given in Tables I and II. The very low SNR in a cell now leads to 72 false measurements per scan.

5. PERFORMANCE OF THE TRACK DETECTOR

5.1. 2-D Results

The LLR of the ML-PMHT for a single run is shown in Figures 5 and 6 for the first 2-D scenario. The plot is centered at the true target location. There are five peaks resulting from path ambiguity. The central peak (the correct one), however, is easily distinguishable from the side peaks. It is also much higher than any peak occurring due to clutter.

We use a simple grid search with 1 km spacing in range, and 20 m/s spacing in velocity to get into the neighborhood of the global maximum of (5). For simplicity, no target feature was used. We then run a local optimization routine from MATLAB using an interior-point algorithm on the highest valued point from the grid search to produce the final state estimate. In the first 2-D scenario this takes approximately 8 seconds per run in MATLAB (faster than real time), and from 10000 Monte Carlo runs the root mean square (RMS) errors for position and velocity at the end of the batch were 40.7 m and 0.7 m/s, respectively. There were no false tracks or missed tracks.

We also applied the MD-MHT [16] to the first 2-D scenario. Using perfect initialization and a sliding window of size 2, the RMS errors from 100 Monte Carlo runs for position and velocity at the end of the run were 83 m and 5.8 m/s, respectively, i.e., significantly larger than the ML-PMHT. An extended Kalman filter was used to update the track with the measurement-path combinations chosen by the algorithm. In the MD-MHT, increasing the window size N_w rapidly increases the computational requirements of the algorithm. The number of hypotheses for a single target scenario depends on the number of paths and measurements and is approximately $(N_{\text{paths}}N_{\text{meas}})^{N_w}$, which quickly becomes intractable.

Using the same grid search method for the second scenario 2, the RMS errors from the ML-PMHT for position and velocity at the end of the batch were 27.2 m and 0.4 m/s, respectively, from 100 Monte Carlo runs, also with no false tracks.

We also ran the first 2-D scenario with different values for the SNR and threshold τ. We chose τ such that P_D remained fixed at 0.34. These results are shown in Table III. In the lowest SNR case (4 dB) the track was detected in each of the 10^4 runs. The algorithm was demonstrated to yield a *track detection probability*, P_{DT}, higher than 95%. Also no false tracks were detected by the algorithm in these 10^4 runs, thus the *probability of false track*, P_{FT}, is at most 10^{-4} for the 15 s time interval. Based on this, the *false track rate* (over 24 hours) is 0.6/day.

5.2. 3-D Results

Figure 7 shows the LLR surface using the true values for azimuth and course. Similarly, Figure 8 shows the LLR surface using the true values for range and speed. We use MATLAB's GlobalSearch algorithm to perform the optimization. From 100 Monte Carlo runs the RMSE values were 3.3 km in position, 54 m in range, and 21 m/s in velocity (in the range direction 0.86 m/s while in the crossrange direction 21 m/s;

TABLE II
Scenario parameters used in the 2-D and 3-D simulations.

	2-D Scenario 1	2-D Scenario 2	3-D Scenario
Resolution cell size	600 m × 10 m/s	15000 m × 10 m/s	1200 m × 20 m/s × 1.2°
Search region size	150 km × 100 m/s	150 km × 100 m/s	150 km × 100 m/s × 90°
Number of cells	2500	100	46875
V	$1.5 \cdot 10^7$ m^2/s	$1.5 \cdot 10^7$ m^2/s	$2.4 \cdot 10^7$ m^2/s × rad
σ_θ	N/A	N/A	0.3°
Amplitude detection threshold τ	2.7	1.7	3.6
P_D for each path	0.34	0.66	0.16
P_{FA} in a cell	0.024	0.24	0.0015
Expected number of false alarms per scan	60	24	72
π_0	0.9776	0.8991	0.9913

TABLE III
Results for various SNR values in the first 2-D scenario from 1000 Monte Carlo runs (results for SNR = 4 dB are from 10000 Monte Carlo runs). The measurement detection threshold τ is chosen such that the single-measurement P_D is fixed at 0.34.

	Cell P_{FA}	Expected number of false alarms (false measurements) per scan	Position RMSE (m)	Velocity RMSE (m/s)	Position CRLB (m)	Velocity CRLB (m/s)
SNR = 10 dB, τ = 4.84	$7 \cdot 10^{-6}$	0.02	32.90	0.5449	33.11	0.5519
SNR = 7 dB, τ = 3.6	0.0015	4	35.30	0.5647	34.36	0.5727
SNR = 6 dB, τ = 3.3	0.0043	11	37.10	0.6037	35.57	0.5929
SNR = 4 dB, τ = 2.73	0.024	60	40.67	0.6760	39.57	0.6595

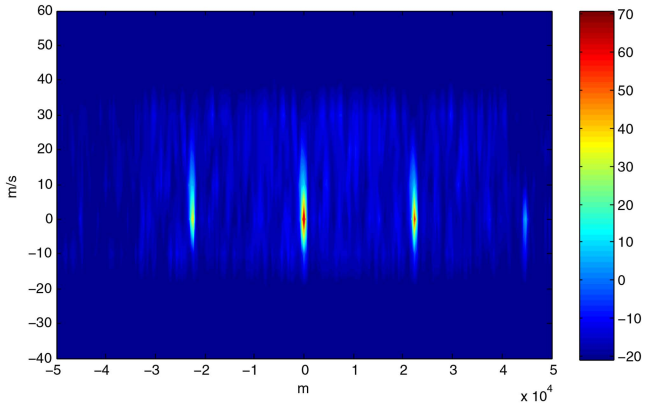

Fig. 5. The log-likelihood ratio centered on the true target state from 2-D scenario 1.

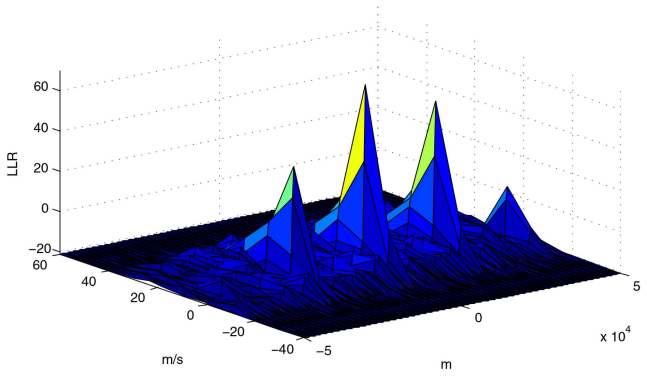

Fig. 6. The log-likelihood ratio centered on the true target state from 2-D scenario 1.

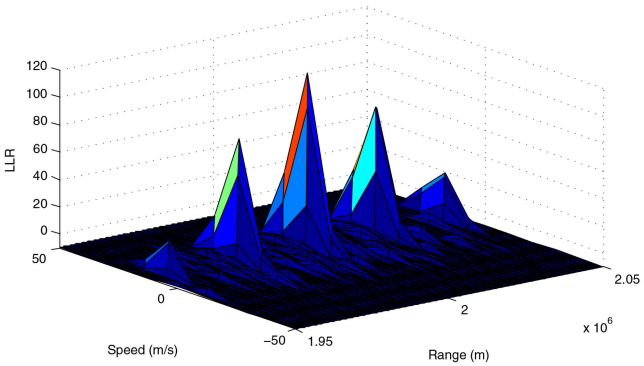

Fig. 7. The log-likelihood ratio at the true values for azimuth and course from the 3-D scenario.

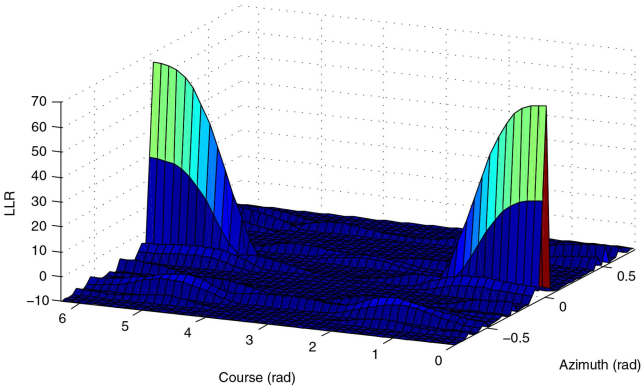

Fig. 8. The log-likelihood ratio at the true values for range and speed from the 3-D scenario.

the latter is due to the fact that the crossrange rate is based on the 0.3° azimuth measurement, which maps to 5 mrad × 2000 km = 10 km crossrange errors, i.e., extremely large).

The algorithm's running time in the 3-D scenario was approximately 2 minutes per run (on 15 s of data) in MATLAB. Therefore, this algorithm can run at least one order of magnitude faster, i.e., it is real time capable if it is implemented in a faster programming language, such as C.

6. MULTIPATH FUSION ML-PMHT CRAMÉR-RAO LOWER BOUND

We develop the Cramér-Rao Lower Bound (CRLB) [3] for the multipath fusion ML-PMHT and show that it is statistically efficient in the first 2-D scenario. We can assume all scans to be independent and also assume the measurements in each scan to be independent. The Fisher Information Matrix (FIM) $\mathbf{J}$ will then be the sum of the FIMs $\mathbf{J}_{i,j}$ of each measurement,

$$\mathbf{J} = \mathrm{E}\{(\nabla_{\mathbf{x}} \ln p[\mathbf{Z} \mid \mathbf{x}])(\nabla_{\mathbf{x}} \ln p[\mathbf{Z} \mid \mathbf{x}])^T\}|_{\mathbf{x}=\mathbf{x}_0} = \sum_{i=1}^{N_w} \sum_{j=1}^{m_i} \mathbf{J}_{i,j} \tag{25}$$

where

$$\mathbf{J}_{i,j} = \mathrm{E}\{(\nabla_{\mathbf{x}(i)} \ln p[\mathbf{z}_j(i) \mid \mathbf{x}(i)]) \cdot (\nabla_{\mathbf{x}(i)} \ln p[\mathbf{z}_j(i) \mid \mathbf{x}(i)])^T\}|_{\mathbf{x}(i)=\mathbf{x}_0(i)} \tag{26}$$

The state vector $\mathbf{x}(i)$ is given by

$$\mathbf{x}(i) = [s_t(i), \dot{s}_t]' \tag{27}$$

where $s_t(i)$ is the target's position at time i, and $\dot{s}_t$ is the target's velocity. The function that transforms $\mathbf{x}(i)$ into the measurement space via the path that reflects both ways off the lower layer only is expressed as (28) with derivatives given by (29) and (30). The functions $f_\ell(\mathbf{x}(i))$ for the other paths (and their derivatives) can be found similarly.

The multipath ML-PMHT likelihood for a single measurement is given by (31). The gradient of the logarithm of this likelihood gives (32), where $\mathbf{D}_\ell(i)$ is the Jacobian of $f_\ell(\mathbf{x}(i))$. Finally, combining equations (26) and (32) gives us the FIM of one measurement, which has to be evaluated numerically, as (33).

$$f_1(\mathbf{x}(i)) = \begin{bmatrix} 4\sqrt{h_1^2 - 2R_\oplus(h_1+R_\oplus)\cos\left(\frac{s_r - s_t(i)}{2R_\oplus}\right) + 2h_1R_\oplus + 2R_\oplus^2} \\ -\dfrac{2\sin\left(\frac{s_r - s_t(i)}{2R_\oplus}\right)(R_\oplus + h_1)}{\sqrt{2R_\oplus h_1 + 2R_\oplus^2 + h_1^2 - 2R_\oplus\cos\left(\frac{s_r - s_t(i)}{2R_\oplus}\right)(R_\oplus + h_1)}}\dot{s}_t(i) \end{bmatrix} \tag{28}$$

$$\frac{\partial}{\partial s_t(i)} f_1(\mathbf{x}(i)) = \begin{bmatrix} -\dfrac{2\sin\left(\frac{s_r - s_t(i)}{2R_\oplus}\right)(R_\oplus + h_1)}{\sqrt{2R_\oplus h_1 + 2R_\oplus^2 + h_1^2 - 2R_\oplus\cos\left(\frac{s_r - s_t(i)}{2R_\oplus}\right)(R_\oplus + h_1)}} \\ \dfrac{\cos\left(\frac{s_r - s_t(i)}{2R_\oplus}\right)(R_\oplus + h_1)\dot{s}_t(i)}{R_\oplus\sqrt{2R_\oplus h_1 + 2R_\oplus^2 + h_1^2 - 2R_\oplus\cos\left(\frac{s_r - s_t(i)}{2R_\oplus}\right)(R_\oplus + h_1)}} \\ -\dfrac{\sin\left(\frac{s_r - s_t(i)}{2R_\oplus}\right)^2(R_\oplus + h_1)^2\dot{s}_t(i)}{[2R_\oplus h_1 + 2R_\oplus^2 + h_1^2 - 2R_\oplus\cos\left(\frac{s_r - s_t(i)}{2R_\oplus}\right)(R_\oplus + h_1)]^{3/2}} \end{bmatrix} \tag{29}$$

$$\frac{\partial}{\partial \dot{s}_t(i)} f_1(\mathbf{x}(i)) = \begin{bmatrix} 0 \\ -\dfrac{2\sin\left(\frac{s_r - s_t(i)}{2R_\oplus}\right)(R_\oplus + h_1)}{\sqrt{2R_\oplus h_1 + 2R_\oplus^2 + h_1^2 - 2R_\oplus\cos\left(\frac{s_r - s_t(i)}{2R_\oplus}\right)(R_\oplus + h_1)}} \end{bmatrix} \tag{30}$$

$$p[\mathbf{z}_j(i) \mid \mathbf{x}(i)] = \frac{\pi_0}{V}p_0^\tau[a_j(i)] + \pi_1 p_1^\tau[a_j(i)]\sum_{\ell=1}^{n_p} p[\mathbf{z}_j(i) \mid \mathbf{x}(i), \ell]P(\ell) \tag{31}$$

$$\nabla_{\mathbf{x}(i)} \ln p(\mathbf{z}_j(i) \mid \mathbf{x}(i)) = \frac{\pi_1 p_1^\tau[a_j(i)]\sum_{\ell=1}^{n_p} P(\ell)|2\pi\mathbf{R}|^{-\frac{1}{2}} e^{-\frac{1}{2}[\mathbf{z}_j(i) - f_\ell(\mathbf{x}(i))]'\mathbf{R}^{-1}[\mathbf{z}_j(i) - f_\ell(\mathbf{x}(i))]}\mathbf{D}_\ell^T(i)\mathbf{R}^{-1}[\mathbf{z}_j(i) - f_\ell(\mathbf{x}(i))]}{\frac{\pi_0}{V}p_0^\tau[a_j(i)] + \pi_1 p_1^\tau[a_j(i)]\sum_{\ell=1}^{n_p} P(\ell)|2\pi\mathbf{R}|^{-\frac{1}{2}} e^{-\frac{1}{2}[\mathbf{z}_j(i) - f_\ell(\mathbf{x}(i))]'\mathbf{R}^{-1}[\mathbf{z}_j(i) - f_\ell(\mathbf{x}(i))]}} \tag{32}$$

$$\mathbf{J}_{i,j} = \int_\tau^\infty \int_V \int \frac{\frac{(\pi_1 p_1^\tau[a_j(i)])^2}{|2\pi\mathbf{R}|}\sum_{\ell=1}^{n_p}\mathbf{A}_\ell(i)\sum_{\ell=1}^{n_p}\mathbf{A}_\ell^T(i)}{\frac{\pi_0}{V}p_0^\tau[a_j(i)] + \pi_1 p_1^\tau[a_j(i)]\sum_{\ell=1}^{n_p} P(\ell)|2\pi\mathbf{R}|^{-\frac{1}{2}} e^{-\frac{1}{2}[\mathbf{z}_j(i) - f_\ell(\mathbf{x}(i))]'\mathbf{R}^{-1}[\mathbf{z}_j(i) - f_\ell(\mathbf{x}(i))]}} d\mathbf{z}_j(i) da_j(i) \tag{33}$$

$$\mathbf{A}_\ell(i) = P(\ell)e^{-\frac{1}{2}[\mathbf{z}_j(i) - f_\ell(\mathbf{x}(i))]'\mathbf{R}^{-1}[\mathbf{z}_j(i) - f_\ell(\mathbf{x}(i))]}\mathbf{D}_\ell^T(i)\mathbf{R}^{-1}[\mathbf{z}_j(i) - f_\ell(\mathbf{x}(i))] \tag{34}$$

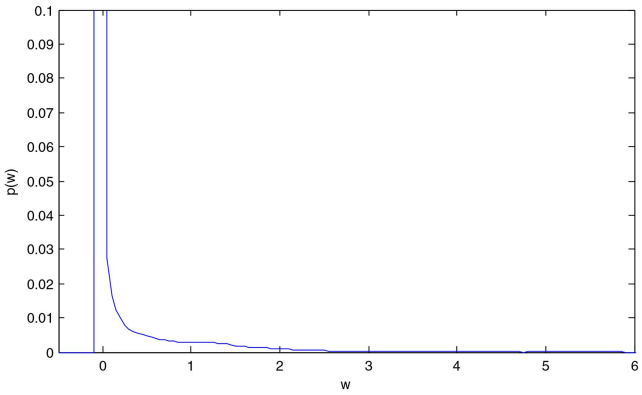

Fig. 9. The pdf of w (a single *clutter* measurement transformed by the multipath LLR).

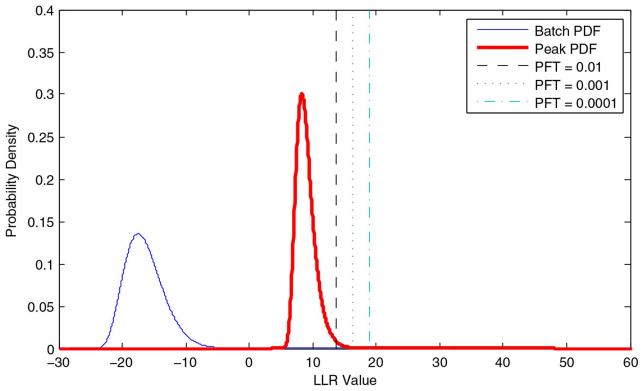

Fig. 10. The batch and peak pdfs (from *clutter*) along with thresholds for several values of P_{FT}.

Using the parameters given in Table I, the CRLB is 39.57 m and 0.6595 m/s for the position and velocity, respectively. From 10000 Monte Carlo runs for the lowest SNR = 4 dB the standard error of the sample variance is 0.5596 m for position, and 0.009327 m/s for velocity [3]. This gives the 95% (2-sigma) intervals of [38.45 m, 40.69 m] and [0.6408 m/s, 0.6782 m/s] for position and velocity, respectively. Since the RMSE values from the *multipath fusion ML-PMHT* (which were 40.67 m and 0.6760 m/s) are within these intervals, it *is a statistically efficient estimator*. We also include the CRLB for different values of the SNR and τ in Table III.

7. FALSE TRACK AND TARGET TRACK DETECTION PROBABILITIES

We use the methods in [19, 20] to determine a threshold for the probability of false track, P_{FT}, and then calculate the probability of track detection, P_{DT}, for the first 2-D scenario with 4 dB SNR presented in Section 4.3.

7.1. Probability of False Track

We begin with the multipath LLR for a single measurement, $\mathbf{z}_j(i)$, and its corresponding amplitude LLR, $\rho_j(i)$,

$$\Lambda_{i,j}[\mathbf{z}_j(i)] = \ln\left\{\pi_0 + \pi_1 V \rho_j(i) \sum_{\ell=1}^{n_p} p[\mathbf{z}_j(i) \mid \mathbf{x}(i), \ell] P[\ell]\right\} \tag{35}$$

and treat $\mathbf{z}_j(i) \in \mathbb{R}^2$ and $\rho_j(i) \in \mathbb{R}^+$ as random variables. Equation (35) is a function that transforms these random variables into a new random variable w,

$$w = \Lambda_{i,j}[\mathbf{z}_j(i)], \quad w \in \mathbb{R} \tag{36}$$

While in [19] it was possible to get a closed-form expression for the pdf of w when using the LLR for a single path ML-PMHT, here we cannot. The sum of exponentials that arises from the multiple paths prevents us from inverting equation (35). We must instead rely on a numerical or empirical approximation of the pdf of w. This empirical pdf of w is shown in Figure 9.

We take the pdf of w and convolve it with itself $N-1$ times to find the pdf for a batch of N measurements from clutter. We refer to this resulting pdf as the "batch" pdf; it is the LLR pdf for a batch of measurements. We use $N = 900$, the expected number of measurements from clutter in one batch of measurements in our scenario. Again, following the methodology of [19], we must use the batch pdf to determine the "peak" pdf; this is the pdf of the maximum sample value from M samples from the batch pdf. This peak pdf is determined from extreme value theory. The determination of M is discussed in [19]; we use $M = 10^7$. The batch and peak pdfs, along with thresholds for several values of P_{FT} are shown in Figure 10.

7.2. Probability of Target Track Detection

Now that we have calculated thresholds using the desired values for P_{FT}, we can use a similar procedure to evaluate P_{DT} for these thresholds using the methods in [20]. We again begin with the multipath LLR for a single measurement given by equation (35), but with $\mathbf{z}_j(i)$ as a Gaussian mixture (for the four paths) random variable (originating from the target) instead of a uniformly distributed random variable (originating from clutter). The approximation of the pdf of a single target measurement transformed by the multipath LLR pdf is shown in Figure 11.

We convolve this pdf with itself $N-1$ times to find the pdf for a batch of N target originated measurements. We use $N = 20$, the expected number of target originated measurements in one batch of $N_w = 15$ scans in our scenario. We do not need to find a peak pdf from this batch pdf; the batch pdf is the peak pdf in this case. The batch pdf and the thresholds calculated in Section 7.1 for several values of P_{FT} are shown in Figure 12. A P_{FT} of 10^{-4} yields $(1 - P_{DT}) = 6 \cdot 10^{-9}$.

8. CONCLUSIONS

We have developed an extension to the single target ML-PMHT to allow for the fusion of data from multiple signal propagation paths. We applied this algorithm to an OTHR scenario. We showed that, with low target

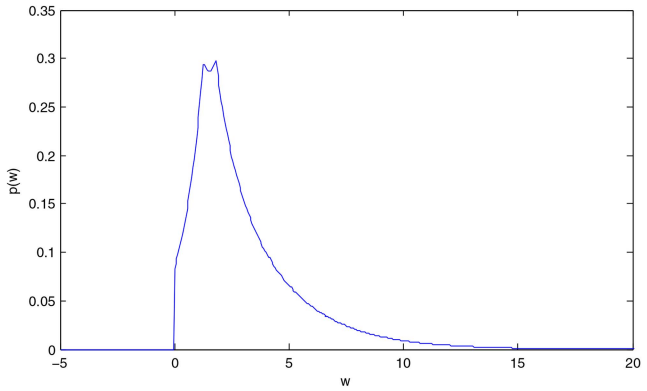

Fig. 11. The pdf of w (a single *target* measurement transformed by the multipath LLR).

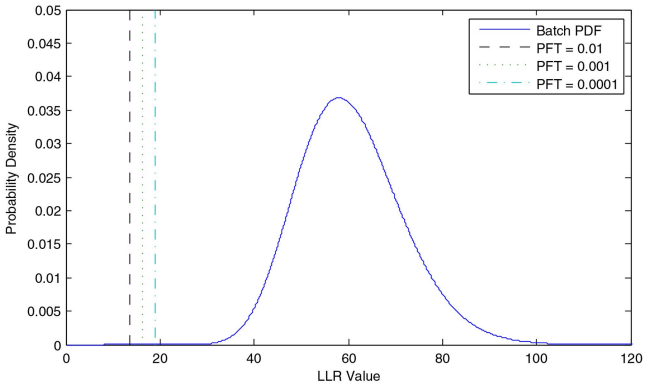

Fig. 12. The batch and peak pdfs (from the *target*) along with thresholds for several values of P_{FT}.

SNR even down to 4 dB post-signal processing, the fusion ML-PMHT has excellent track detection and accuracy in such a scenario and is statistically efficient. Consequently, the ML-PMHT holds great promise in increasing the sensitivity and robustness of the next generation OTHR.

The results indicate that the ML-PMHT can yield very high P_{DT} (probability of track detection) and very low P_{FT} (probability of false track). Future work would include using a more accurate ionosphere model.

REFERENCES

[1] R. H. Anderson, and J. L. Krolik
Multipath track association for over-the-horizon radar using a bootstrapped statistical ionospheric model.
In *Conference Record of the Thirty-Third Asilomar Conference on Signals, Systems, and Computers*, 1999, 8–14.

[2] R. H. Anderson, and J. L. Krolik
Track association for over-the-horizon radar with a statistical ionospheric model.
IEEE Transactions on Signal Processing, 50, 11 (2002), 2632–2643.

[3] Y. Bar-Shalom, X.-R. Li, and T. Kirubarajan
Estimation with Applications to Tracking and Navigation.
New York: Wiley, 2001.

[4] Y. Bar-Shalom, P. K. Willett, and X. Tian
Tracking and Data Fusion.
Storrs, CT: YBS Publishing, 2011.

[5] W. R. Blanding, P. K. Willett, and Y. Bar-Shalom
Offline and real-time methods for ML-PDA track validation.
IEEE Transactions on Signal Processing, 55, 5 (May 2007), 1994–2006.

[6] S. B. Colegrove, and S. J. Davey
The probabilistic data association filter with multiple non-uniform clutter regions.
In *The Record of the IEEE 2000 International Radar Conference*, 2000, 65–70.

[7] S. B. Colegrove, and S. J. Davey
PDAF with multiple clutter regions and target models.
IEEE Transactions on Aerospace and Electronic Systems, 39, 1 (Jan. 2003), 110–124.

[8] S. B. Colegrove, S. J. Davey, and B. Cheung
PDAF versus PMHT performance on OTHR data.
In *Proceedings of the International Radar Conference, 2003*, Sep. 2003, 560–565.

[9] S. V. Fridman, and L. J. Nickisch
SIFTER: signal inversion for target extraction and registration.
Radio Science, 39, 1 (2004).

[10] H. Lan, Y. Liang, Q. Pan, F. Yang, and C. Guan
An EM algorithm for multipath state estimation in OTHR target tracking.
IEEE Transactions on Signal Processing, 62, 11 (2014), 2814–2826.

[11] D. J. Percival, and K. A. B. White
Multihypothesis fusion of multipath over-the-horizon radar tracks.
In *Proceedings of SPIE 3373, Signal and Data Processing of Small Targets*, 1998.

[12] G. W. Pulford, and R. J. Evans
A multipath data association tracker for over-the-horizon radar.
IEEE Transactions on Aerospace and Electronic Systems, 34, 4 (Oct. 1998), 1165–1183.

[13] M. G. Rutten, S. Maskell, M. Briers, and N. J. Gordon
Multipath track association for over-the-horizon radar using Lagrangian relaxation.
In *Proceedings of SPIE Signal and Data Processing of Small Targets*, 2004.

[14] M. G. Rutten, and D. J. Percival
Comparison of track fusion with measurement fusion for multipath OTHR surveillance.
In *Proceedings of the 4th International Conference on Information Fusion*, 2001.

[15] M. G. Rutten, and D. J. Percival
Joint ionospheric and target state estimation for multipath OTHR track fusion.
In *Proceedings of SPIE Signal and Data Processing of Small Targets*, 2001.

[16] T. Sathyan, T.-J. Chin, S. Arulampalam, and D. Suter
A multiple hypothesis tracker for multitarget tracking with multiple simultaneous measurements.
IEEE Journal of Selected Topics in Signal Processing, 7, 3 (Jun. 2013), 448–460.

[17] S. Schoenecker, P. Willett, and Y. Bar-Shalom
Maximum likelihood probabilistic multi-hypothesis tracker applied to multistatic sonar data sets.
In *Proceedings of SPIE Conference on Signal Processing, Sensor Fusion, and Target Recognition*, Mar. 2011.

[18] S. Schoenecker, P. Willett, and Y. Bar-Shalom
ML-PDA and ML-PMHT: Comparing multistatic sonar trackers for VLO targets using a new multitarget implementation.
IEEE Journal of Oceanic Engineering, 39, 2 (Apr. 2014), 303–317.

[19] S. Schoenecker, P. Willett and Y. Bar-Shalom
Extreme-value analysis for ML-PMHT, part 1: target trackability.
IEEE Transactions on Aerospace and Electronic Systems, (2014 in print).

[20] S. Schoenecker, P. Willett and Y. Bar-Shalom
Extreme-value analysis for ML-PMHT, part 2: false track probability.
IEEE Transactions on Aerospace and Electronic Systems, (2014 in print).

Kevin Romeo received his B.S. degree in 2009 from the Department of Electrical and Computer Engineering, University of Connecticut, Storrs, USA in engineering physics. He is currently working towards the completion of his PhD degree in Electrical Engineering from the University of Connecticut. His main research interests lie in the areas of target tracking and detection.

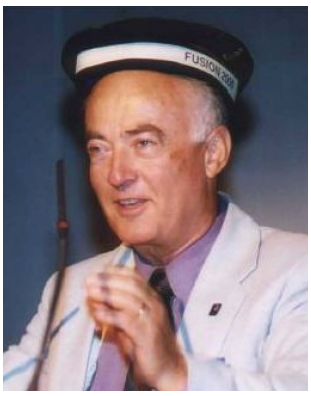

Yaakov Bar-Shalom was born on May 11, 1941. He received the B.S. and M.S. degrees from the Technion, Israel Institute of Technology, in 1963 and 1967 and the Ph.D. degree from Princeton University in 1970, all in electrical engineering. From 1970 to 1976 he was with Systems Control, Inc., Palo Alto, California. Currently he is Board of Trustees Distinguished Professor in the Dept. of Electrical and Computer Engineering and Marianne E. Klewin Professor in Engineering at the University of Connecticut. He is also Director of the ESP (Estimation and Signal Processing) Lab. His current research interests are in estimation theory, target tracking and data fusion. He has published over 500 papers and book chapters in these areas and in stochastic adaptive control. He coauthored the monograph Tracking and Data Association (Academic Press, 1988), the graduate texts Estimation and Tracking: Principles, Techniques and Software (Artech House, 1993; translated into Russian, MGTU Bauman, Moscow, Russia, 2011), Estimation with Applications to Tracking and Navigation: Algorithms and Software for Information Extraction (Wiley, 2001), the advanced graduate texts Multitarget-Multisensor Tracking: Principles and Techniques (YBS Publishing, 1995), Tracking and Data Fusion (YBS Publishing, 2011),and edited the books Multitarget-Multisensor Tracking: Applications and Advances (Artech House, Vol. I, 1990; Vol. II, 1992; Vol. III, 2000). He has been elected Fellow of IEEE for "contributions to the theory of stochastic systems and of multi-target tracking." He has been consulting to numerous companies and government agencies, and originated the series of Multitarget-Multisensor Tracking short courses offered via UCLA Extension, at Government Laboratories, private companies and overseas. During 1976 and 1977 he served as Associate Editor of the IEEE Transactions on Automatic Control and from 1978 to 1981 as Associate Editor of Automatica. He was Program Chairman of the 1982 American Control Conference, General Chairman of the 1985 ACC, and Co-Chairman of the 1989 IEEE International Conference on Control and Applications. During 1983–87 he served as Chairman of the Conference Activities Board of the IEEE Control Systems Society and during 1987–89 was a member of the Board of Governors of the IEEE CSS. He was a member of the Board of Directors of the International Society of Information Fusion (1999–2004) and served as General Chairman of FUSION 2000, President of ISIF in 2000 and 2002 and Vice President for Publications in 2004–13. In 1987 he received the IEEE CSS Distinguished Member Award. Since 1995 he is a Distinguished Lecturer of the IEEE AESS and has given numerous keynote addresses at major national and international conferences. He is co-recipient of the M. Barry Carlton Award for the best paper in the IEEE Transactions on Aerospace and Electronic Systems in 1995 and 2000 and recipient of the 1998 University of Connecticut AAUP Excellence Award for Research. In 2002 he received the J. Mignona Data Fusion Award from the DoD JDL Data Fusion Group. He is a member of the Connecticut Academy of Science and Engineering. In 2008 he was awarded the IEEE Dennis J. Picard Medal for Radar Technologies and Applications, and in 2012 the Connecticut Medal of Technology. He has been listed by academic.research.microsoft (top authors in engineering) as #1 among the researchers in Aerospace Engineering based on the citations of his work.

Peter Willett has been a faculty member in the Electrical and Computer Engineering Department at the University of Connecticut since 1986. Since 1998 he has been a Professor, and since 2003 an IEEE Fellow. He has published 187 journal and 395 conference proceedings articles. His primary areas of research have been statistical signal processing, detection, machine learning, communications, data fusion, and tracking. He is Editor-In-Chief of IEEE Signal Processing Letters and is IEEE Aerospace and Electronic Systems Vice President for Publications. He was editor-in-chief for IEEE Transactions on Aerospace and Electronic Systems from 2006–2011. For 1998–2005 he was associate editor for three active journals { IEEE Transactions on Aerospace and Electronic Systems (for Data Fusion and Target Tracking) and IEEE Transactions on Systems, Man, and Cybernetics, parts A and B. He is remains associate editor for the IEEE AES Magazine, and ISIF's Journal of Advances in Information Fusion, and is a member of the editorial board of IEEE's Special Topics in Signal Processing journal and a senior editor for IEEE Signal Processing Letters. He is a member of the IEEE AESS Board of Governors and of the IEEE Signal Processing Society's Sensor-Array and Multichannel (SAM) technical committee (and is now Vice Chair).